communications physics

ARTICLE

https://doi.org/10.1038/s42005-022-01110-y OPEN

Ultrafast signatures of spin and orbital order in antiferromagnetic α-Sr_2CrO_4

Min-Cheol Lee[1✉], Connor Occhialini[2], Jiarui Li[2], Zhihai Zhu[2,3], Nicholas S. Sirica[1], L. T. Mix[1], Soyeun Kim[4,5], Dmitry A. Yarotski[1], Riccardo Comin[2] & Rohit P. Prasankumar[1✉]

The antiferromagnetic Mott insulator α-Sr_2CrO_4 possesses multiple spin and orbital ordered phases, but their unique interplay is still relatively unexplored. Here, we used femtosecond optical spectroscopy to study ultrafast spin and orbital ordering dynamics in α-Sr_2CrO_4 through their non-equilibrium response to photoexcitation. By varying the pump photon energy, we selectively drove inter-site spin hopping between neighboring Cr t_{2g} orbitals and charge transfer-type transitions between oxygen $2p$ and Cr e_g orbitals. The resulting transient reflectivity dynamics revealed temperature-dependent anomalies across the Néel temperature for spin ordering as well as the transition temperatures linked to different types of orbital order. Our results reveal distinct relaxation timescales for spin and orbital orders in α-Sr_2CrO_4 and provide experimental evidence for the phase transition at T_O, possibly related to antiferro-type orbital ordering.

[1] Center for Integrated Nanotechnologies, Los Alamos National Laboratory, Los Alamos, NM, USA. [2] Department of Physics, Massachusetts Institute of Technology, Cambridge, MA, USA. [3] Beijing National Laboratory for Condensed Matter Physics, Institute of Physics, Chinese Academy of Sciences, Beijing 100190, China. [4] Department of Physics, University of Illinois at Urbana-Champaign, Urbana 61801 IL, USA. [5] Materials Research Laboratory, University of Illinois at Urbana-Champaign, Urbana 61801 IL, USA. ✉email: mincheol.chris.lee@gmail.com; rpprasan@alum.mit.edu

Transition metal (TM) compounds provide a versatile platform for exploring a wide variety of strongly correlated phenomena, such as high-T_C superconductivity, multiferroicity, or unusual magnetism[1–3]. These phenomena are accompanied by various types of charge, spin and orbital orders, arising from competition between interactions such as the local crystal field, inter-site exchange interactions, spin-orbit coupling and on-site Coulomb repulsion[3]. Several phase transitions can occur in a single compound at different temperatures, as observed in multi-orbital systems with partially filled *d*-shells, including cuprates[4], manganites[5,6], and ruthenates[7].

Chromates are an intriguing member of this class of materials, due to their active degrees of freedom (DOFs), multiple electronic symmetry breaking pathways, and competing order parameters. The case of α-Sr_2CrO_4 is particularly interesting, as it has been shown to exhibit multiple spin and orbital ordering transitions in the Mott insulating ground state (Fig. 1(a))[8–12]. α-Sr_2CrO_4 presents a unique electronic configuration, with two electrons in t_{2g} orbitals and total spin of $S = 1$. Recent resonant X-ray scattering (RXS)[8] and neutron powder diffraction studies[9] demonstrated antiferromagnetic (AFM) order by tracking a magnetic Bragg peak below the Néel temperature ($T_N = 112$ K), consistent with the temperature (T)-dependent magnetic susceptibility[10]. The RXS study also revealed another in-plane order below $T_S = 50$ K[8], which was attributed to stripe-type spin-orbital order in the d_{yz}/d_{zx} orbital sub-manifold (Fig. 1(a)). α-Sr_2CrO_4 also manifests a signature of a broad transition around $T_O = 140$ K in the specific heat, which is likely unrelated to spin order, as the magnetic susceptibility follows a typical Curie-Weiss law across T_O[10]. The exact origin of this feature has not been unveiled yet, though it was suggested to arise from a distinct antiferro(AF)-type orbital order in the d_{yz} and d_{zx} orbitals (Fig. 1(a)), as in Sr_2VO_4[10,13]. Therefore, more experimental insight is needed to unravel the origin of this phase transition at T_O above the Néel temperature.

In this context, ultrafast optical spectroscopy (UOS) is a powerful tool for providing insight into the intertwined spin and orbital DOFs in TM compounds[14]. By using femtosecond (fs) photoexcitation to drive the system out of equilibrium, the interplay among the competing charge, spin and orbital DOFs can be disentangled via their different timescales for returning to the initial ground state, as exemplified in previous studies of various TM oxides[15–22]. However, to the best of our knowledge this technique has not yet been used to study α-Sr_2CrO_4, providing an exciting opportunity to shed light on the origin of the various order parameters present in this system.

In this work, we thus investigate the non-equilibrium dynamics of spin and orbital order in α-Sr_2CrO_4 by measuring the transient changes in reflectivity at 1.55 eV after femtosecond optical photoexcitation. By varying the pump photon energy, we can selectively drive specific microscopic processes that trigger clear T-dependent anomalies across the spin and orbital order temperatures. Photoexcitation at 1.0 eV directly perturbs spin and orbital order by inducing spin hopping between neighboring Cr^{4+} ions. In contrast, 3.1 eV photons excite carriers through a charge-transfer-type transition (which does not directly affect spin/orbital order), yet the resulting relaxation dynamics are still influenced by the existing spin and orbital ordered states. Our results thus show that UOS is sensitive to all three of the spin and orbital ordering transitions that have been previously measured via other techniques[8,10] through their distinct timescales[14]. Furthermore, we provide experimental evidence for the existence of a phase transition at T_O, with a close relation to the stripe-type spin-orbital order below T_S.

Results and discussion

Experimental description. We measured the time-resolved photoinduced changes in reflectivity on an epitaxially grown, 100 nm thick *c*-axis oriented film of α-Sr_2CrO_4, which is usually hard to synthesize in bulk single crystalline form[8]. Our experiments were based on a 250 kHz femtosecond (fs) regenerative amplifier producing ~ 100 fs pulses at 1.55 eV, used to probe the transient response and also to pump an optical parametric amplifier that generated the 1.0 eV pump pulses. A beta-barium borate (BBO) crystal was used to obtain the 3.1 eV pump pulses by frequency doubling the fundamental 1.55 eV pulses. We used a near normal

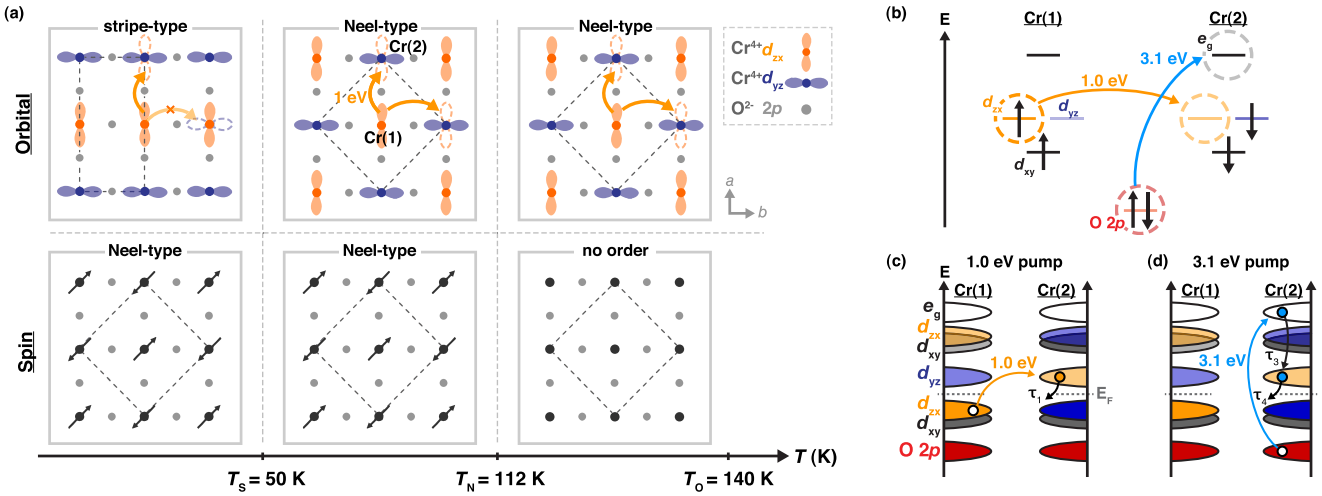

Fig. 1 Spin and orbital order in α-Sr_2CrO_4. a Schematic diagrams of the spin- and orbital-ordered ground state in α-Sr_2CrO_4, showing different types of antiferro-type spin ordering and d_{yz}/d_{zx} orbital ordering. We note that the four-lobed shapes of the *d*-orbitals are projected into the *ab*-plane. Arrows indicate possible 1 eV transitions from occupied (filled shapes) to unoccupied (dotted shapes) orbital states in a given ordered phase; transitions from Cr(1) to Cr(2) ions are shown for simplicity, but the reverse can also occur. **b** Energy (E) levels and orbital structures on neighboring sites with Cr(1) and Cr(2) ions at a temperature (T) below the Néel temperature (T_N): $T \leq T_N$. The *d*-*d* transitions between d_{zx} orbitals from Cr(1) to Cr(2) (or between d_{yz} orbitals from Cr(2) to Cr(1)) correspond to hopping energies of 1.0 eV. 3.1 eV excitation drives a charge-transfer-type transition from O 2*p* to Cr e_g orbitals. The relevant electronic structures are displayed along with photoexcitation at (**c**) 1.0 eV and (d) 3.1 eV. On-site transitions from O 2*p* to Cr e_g states are possible at both Cr(1) and Cr(2) sites.

incident geometry for both pump and probe beams, which were linearly cross-polarized along the two equivalent in-plane a-axes (since α-Sr_2CrO_4 has tetragonal symmetry). The fluence of the 1.0 eV (3.1 eV) pump pulses was 400 (800) μJ cm^{-2}, generating 0.022 (0.034) carriers/Cr site and a lattice temperature increase < 5 K. We measured the time-resolved reflectivity data up to $t = 250$ picoseconds (ps), and verified that the measured response was linear with pump fluence up to ~ 1 mJ cm^{-2} for both 1.0 eV and 3.1 eV pumping.

To observe non-equilibrium spin and orbital ordering dynamics, we used our 1.0 eV and 3.1 eV pump pulses to drive specific transitions in the electronic structure of α-Sr_2CrO_4. Two electrons occupy Cr^{4+} t_{2g} states in α-Sr_2CrO_4, leading to a reversed crystal splitting effect that lifts their degeneracy[9,23]. This results in a lower energy for the d_{xy} orbital compared to those of the d_{yz}/d_{zx} orbitals (Fig. 1(b)). Theoretical calculations of the ground state orbital structure also revealed an AF pattern in the occupancy of d_{zx} and d_{yz} orbitals on neighboring Cr^{4+} ions (Cr(1) and Cr(2)) below T_O, in addition to AF spin ordering below T_N[12,23]. These AF spin and orbital orderings produce different partial densities of states on neighboring Cr ions, resulting in an energy scale of 1.0 eV for inter-site spin hopping from Cr(1) to Cr(2) (Cr(2) to Cr(1)) sites between d_{zx} (d_{yz}) orbitals, as indicated by the orange arrows in Fig. 1[23] (see the supplementary material for additional experimental details in Supplementary Note 1). Additionally, charge transfer-type transitions between neighboring oxygen $2p$ and Cr e_g orbitals occur at higher energy scales (~3 eV). We note that these assignments also agree with previous optical conductivity data[11] and our data (see the supplementary material for additional experimental details in Supplementary Note 2 with Fig. S2), showing clear peaks at these photon energies. In our experiments, therefore, 1.0 eV photoexcitation directly perturbs spin and orbital order, while 3.1 eV photoexcitation creates carriers whose dynamics are influenced by the existing spin and orbital orders as they relax from higher energy states. We tracked the resulting dynamics with a probe photon energy of 1.55 eV, set below the charge transfer (CT) gap energy of 2.0 eV[11] to give general sensitivity to dynamics in all t_{2g} orbitals. Even though the CT transition can contribute to the dynamics measured at 1.55 eV, it too is sensitive to spin and orbital order, as 2 eV corresponds to the transition from O $2p$ to Cr t_{2g} states (Fig. 4 in ref. [23]).

Figure 2 shows T-dependent transient reflectivity ($\Delta R/R$) data for both pump photon energies, revealing dynamics on both fast (sub-ps) and relatively slow timescales. After 1.0 eV photoexcitation, a step-like feature appears immediately after time $t \sim 0$ ps at high temperatures, as exemplified at 180 K, while an additional decaying component arises at low temperatures, as seen at 20 K. In contrast, while the 1.0 eV pump data shows a monotonic decay after $t \sim 0$ ps (Fig. 2(a)), the dynamics are more complicated after 3.1 eV photoexcitation, displaying a sharp peak at $t = 0.2$ ps as well as a slowly rising component up to $t \sim 4$ ps (Fig. 2(b)). Finally, there is a slow decay at low temperatures and long time delays after both 1.0 eV and 3.1 eV photoexcitation. We note that the periodic oscillations at a frequency of 22 GHz in the transient reflectivity after 3.1 eV photoexcitation are due to optically driven acoustic phonons (see the supplementary material for additional experimental details)[24]; this is well established and will not be discussed further here.

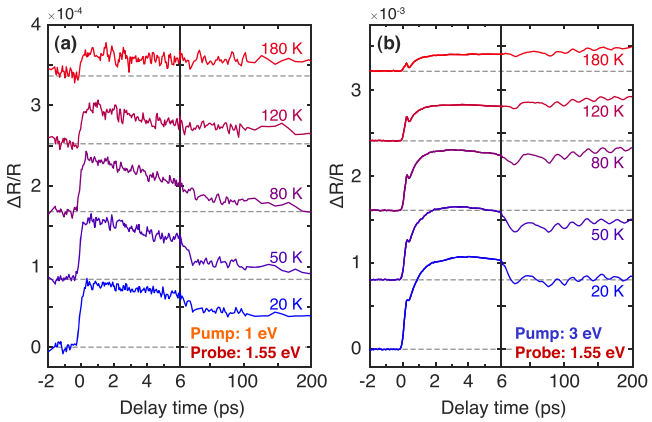

Fig. 2 Photoinduced time-resolved changes in reflectivity ($\Delta R/R$) in α-Sr_2CrO_4. We measured $\Delta R/R$ at 1.55 eV after (**a**) 1.0 eV and (**b**) 3.1 eV photoexcitation at various temperatures.

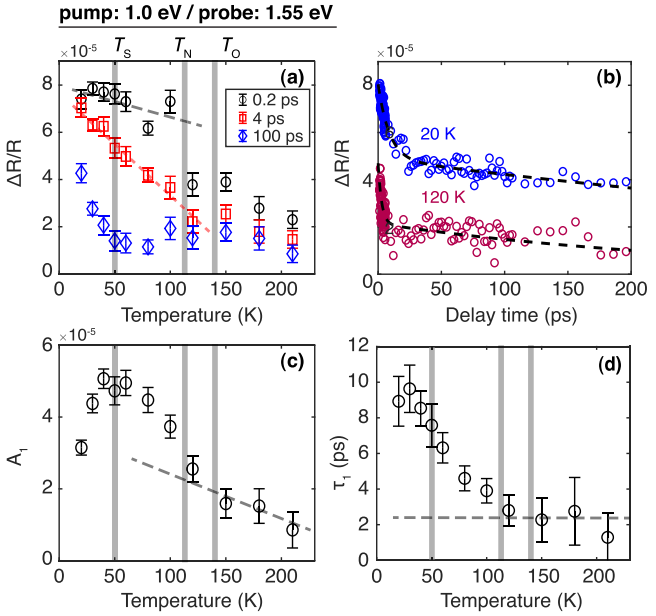

Fig. 3 Analysis of the temperature-dependent reflectivity transients ($\Delta R/R$) after 1.0 eV photoexcitation. a $\Delta R/R$ at time delays of 0.2 ps (black circles), 4 ps (red squares), and 100 ps (blue diamonds). **b** Transient reflectivity data at temperature $T = 20$ K (blue circles) and 120 K (purple circles) along with fits using bi-exponential decay functions (dashed lines). The temperature dependence of the (**c**) amplitude A_1 and (**d**) decay time τ_1 of the fast component extracted from our fits. The solid grey lines indicate the transition temperatures of the stripe-type order (T_S), antiferro-type spin order (T_N), and antiferro-type orbital order (T_O), respectively. The error bars were calculated as described in Methods.

Dynamics after 1.0 eV photoexcitation. For more insight, we plotted the T-dependence of the $\Delta R/R$ signal at different time delays after 1.0 eV pumping in Fig. 3(a). $\Delta R/R$ at the peak ($t = 0.2$ ps) and $t = 4$ ps clearly deviates from the low-T linear behavior across T_N. In contrast, at longer timescales of t = 100 ps, we observe an increase in the $\Delta R/R$ signal below the stripe-type ordering temperature ($T_S = 50$ K). This suggests that the dynamics at short and long timescales after 1.0 eV photoexcitation are related to Néel spin order and stripe-type spin-orbital order, respectively.

To quantify the timescale for the recovery of magnetic order, we fit our data with a bi-exponential decay function, $\Delta R(t)/R = A_1 \exp(-t/\tau_1) + A_2 \exp(-t/\tau_2)$, from $t = 0.2$ ps to 200 ps, as shown in Fig. 3(b) (see Supplementary Note 3 for the detail and Fig. S3 for the fitting results at all measured temperatures.) Both the amplitude A_1 (Fig. 3(c)) and decay time τ_1 (Fig. 3(d)) of the fast component clearly show a gradual

increase below T_N. Near the lowest temperatures, $\tau_1 \sim 10$ ps, revealing the timescale on which AFM order recovers after 1.0 eV excitation. Previous work on antiferromagnetic TM oxides has demonstrated that this time constant is linked to spin-lattice relaxation, i.e. photoexcited electrons rapidly transfer their energy to the lattice, which in turn equilibrates with spins on a timescale given by τ_1[19,25]; this is consistent with our data, and indicates that AFM order restricts carrier hopping below T_N (Fig. 1(a)). Such dynamics of τ_1 does not appear in the $\Delta R/R$ data following 3.1-eV pump, as the spin order is not likely to be destroyed by photoexcitation to Cr e_g bands. We also found that τ_2 exhibits a slower decay time (~200 ps) above T_S (see Fig. S4(b)), likely due to residual lattice heating. However, below T_S, τ_2 increases up to ~500 ps, which may be linked to a structural change occurring concurrently with the appearance of stripe-type spin-orbital order (see Fig. S5 in Supplementary Note 4).

Dynamics after 3.1 eV photoexcitation. In contrast with the transient reflectivity measured after 1.0 eV photoexcitation, which exhibited a relatively simple exponential recovery, the dynamics after 3.1 eV photoexcitation are more complex. Fig. 2(b) reveals three distinct timescales, including (1) the initial sharp peak at $t = 0.2$ ps, followed by (2) an increase up to $t \sim 4$ ps and (3) a subsequent decay on longer timescales. Fig. 4(a) shows $\Delta R/R$ as a function of T at time delays corresponding to these features. While the initial dynamics at $t = 0.2$ ps shows only small T-dependent anomalies, $\Delta R/R$ at 4 ps and 100 ps changes across T_S, similar to the results after 1.0 eV excitation.

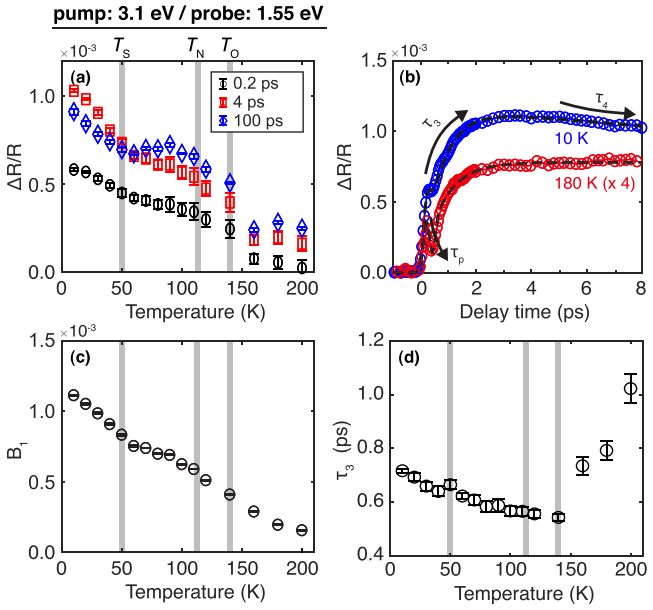

Fig. 4 Analysis of the temperature-dependent reflectivity transients ($\Delta R/R$) after 3.1 eV photoexcitation. a $\Delta R/R$ at time delays of 0.2 ps (black circles), 4 ps (red squares), and 100 ps (blue diamonds). We also plot the amplitude B_1 (orange circles) obtained from our curve fits. **b** Transient reflectivity data at temperature $T = 20$ K (blue circles) and 180 K (red circles), along with fits using the model described in the text. The data and fit curve at 180 K are scaled up by a factor of four for clear comparison. **c** The rise time (τ_3) and (d) decay time (τ_4) obtained from the ultrafast dynamics in (b), revealing a clear anomaly across the antiferro-type orbital ordering temperature $T_O = 140$ K. The error bars were calculated as described in Methods.

For a more quantitative analysis, we fit the data up to 25 ps with a model function:

$$\frac{\Delta R}{R}(t) = S(t) \times \left(1 - \exp\left(-\frac{t}{\tau_3}\right)\right) \times \left(B_1 \exp\left(-\frac{t}{\tau_4}\right)\right) + C \exp\left(\frac{-(t-t_0')^2}{\tau_p}\right). \quad (1)$$

While a simple two-exponential decay model was sufficient to fit the 1.0 eV data, for the 3.1 eV data we used equation (1), particularly to account for the relatively slow rising dynamics. In this model, $S(t) = (1 + erf(t/\tau_0))/2$ is a step-function representing the convolution of the material response with the pulse duration of $\tau_0 \sim 100$ fs. We use $1 - \exp(-t/\tau_3)$ to fit the slow rising dynamics with a rise time τ_3, and $B\exp(-t/\tau_4)$ to fit the subsequent decay with amplitude B and decay time τ_4. The remaining part, $C_1 \exp(-(x - t_0')/\tau_p)^2)$, is used to fit the initial peak at $t_0' \sim 0.2$ ps. The fitting results at $T = 10$ and 180 K are displayed in Fig. 4(b) with the raw data, showing that our model can accurately represent the complex dynamics triggered by 3.1 eV pumping (see Supplementary Note 5 for the fitting detail and Fig. S6 for the fitting results at all temperatures).

The initial sharp peak may originate from several different processes, including electron-electron scattering among the photoexcited carriers[26] and two-photon absorption; additional measurements are required to conclusively determine its origin. Regardless, the initial charge transfer-type excitation between O $2p$ to Cr e_g states on neighboring ions driven by 3.1 eV photoexcitation should not directly influence magnetic or orbital order on ultrafast timescales, because neither the initial nor the final state are involved with the spin and orbital order in the Cr t_{2g} states (Fig. 1(d)). This is why the dynamics after 1 eV photoexcitation characterized by τ_1 do not appear in the $\Delta R/R$ data following 3.1 eV pumping, as spin order is not destroyed by photoexcitation to Cr e_g bands.

After the initial peak, the slow rise denoted by τ_3 (Fig. 4(b)) is due to relaxation of the photoinduced carriers from their initial e_g levels into the t_{2g} states examined by our 1.55 eV probe pulse, as indicated by the upper black arrow in Fig. 1(d)). This slow rising component does not appear in the 1.0 eV data (Fig. 2(a)), since our 1.55 eV probe energy is higher than that of the 1.0 eV pump. Despite a gradual change in the amplitude B_1 (Fig. 4(c)), the relevant rise time, τ_3, shows a clear anomaly across $T_O = 140$ K (Fig. 4(d)), a transition temperature that has been observed only once before via specific heat measurements[10]. This suggests that the orbital configuration changes below T_O, which can influence carrier relaxation into the conduction band minima originating from Cr t_{2g} orbitals.

For further insight into the orbital configuration, we refer to previous theoretical calculations based on a Kugel-Khomskii model (Fig. 4(a) in[8]). Considering the exchange interactions between the neighboring spins and orbitals within t_{2g} states, two different antiferro-type orbital orderings in the d_{yz} and d_{zx} states with Néel-type and stripe-type patterns can exist (Fig. 1(a)), depending on the next-nearest-neighbor exchange coupling. These calculations confirmed that the stripe-type orbital order has a lower energy, which should be accompanied by a reconfiguration of the spin degrees of freedom. This agreed with RXS data showing a scattering signal consistent with stripe-type order at the lowest temperatures[8], as well as muon spin rotation data showing a second oscillatory component that may be due to coexisting stripe-type spin order[27]. These results therefore suggested that stripe-type spin-orbital order is the ground state, but AF-type orbital order can also exist in α-Sr_2CrO_4, depending on inter-site interactions between Cr ions.

The appearance of stripe-type spin-orbital order below T_S causes the amplitude A_1, associated with the spin demagnetization dynamics triggered by 1.0 eV pumping, to be suppressed (Fig. 3(c)). This occurs because the probability of inter-site transitions driven by 1.0 eV photoexcitation between the same spin-polarized d_{yz} (or d_{zx}) orbitals at the nearest Cr ions in the stripe-type spin-orbital ordered phase is half of that at higher temperatures, as with τ_4 (Fig. 1(a)). However, the relevant decay time τ_1 for spin relaxation does not change abruptly across T_S, suggesting a persistent nature of the Néel-type spin order that is stable at all temperatures below T_N, though it may be accompanied by stripe-type spin order below T_S[27]. This corresponds to the previous RXS results, showing a gradual development of the Néel-type magnetic Bragg peak across T_S[8].

Finally, at higher temperatures, the T-dependent anomalies in τ_3 and τ_4 across $T_O = 140$ K most likely originate from the phase transition into the AF-type orbital ordered state. Assuming that there is no orbital order above T_O, the electronic structure for $T > T_O$ will differ from the orbital-ordered state below T_O. This is supported by the fact that the c-axis lattice constant in the CrO_6 octahedral structure decreases below T_O, as shown in Fig. S5[9](See the supplementary material for additional experimental details). Such distortions in the octahedral structure can change the hybridization strength between t_{2g} and e_g orbitals[28], which in turn affects the on-site relaxation of photoinduced carriers from e_g states to t_{2g} states after 3.1 eV photoexcitation (Fig. 1(d)). In other words, an increase in t_{2g}-e_g hybridization will enable photoexcited electrons in the e_g bands to scatter into the t_{2g} bands more effectively, decreasing τ_3 below T_O. Simultaneously, the photo-excited holes will hop from the O_{2p} oxygen states to either Cr(1) or Cr(2) ions, facilitating both on-site and inter-site recombination with the excess electrons in the t_{2g} bands (both processes contribute to τ_4). These considerations thus give us a general picture of carrier dynamics in α-Sr_2CrO_4 (and its sensitivity to orbital order) after 3.1 eV photoexcitation.

Conclusions

In conclusion, we used femtosecond optical spectroscopy to track non-equilibrium carrier dynamics in α-Sr_2CrO_4, revealing clear temperature-dependent anomalies across the spin and orbital ordering temperatures. These experimental results are consistent with a theoretical prediction[8] of two possible orbital configurations in the d_{yz} and d_{zx} states, i.e. Néel-type order below T_O that turns into stripe-type order below T_S. Overall, our results underline the ability of ultrafast optical spectroscopy to distinguish spin and orbital orders through their timescales for coupling to the electronic structure in complex materials.

Methods

The time-resolved photoinduced changes in reflectivity were measured on an epitaxially grown 100 nm thick c-axis oriented film of α-Sr_2CrO_4. We used a 250 kHz femtosecond regenerative amplifier producing ~100 fs pulses at 1.55 eV to probe the transient response. The 1.55 eV pulses were also used to pump an optical parametric amplifier that generated the 1.0 eV pump pulses. We used a beta-barium borate (BBO) crystal to obtain the 3.1 eV pump pulses by frequency doubling the fundamental 1.55 eV pulses. We used a near normal incident geometry for both pump and probe beams, which were linearly cross-polarized along the two equivalent in-plane a-axes of tetragonal α-Sr_2CrO_4. We measured the time-resolved reflectivity data up to $t = 250$ ps. We used an UV-VIS spectrometer to obtain the reflectivity data at room temperature. The light polarization was set to be perpendicular to the c-axis. We then transformed the reflectivity to optical conductivity using a Kramers-Kronig analysis. The error bars in (Figs. 3a and 4a) are calculated by using the deviations between the raw data taken at the neighboring time delays within 100 fs. The error bars in (Figs. 3c, d and Fig. 4c, d) in the main text and Fig. S4a, b, Fig. S7a–d and Fig. S8c–f were calculated by curve fitting to the raw data with 95% confidence bounds. We also observed coherent oscillatory signals in the 3.1 eV pump and 1.55 eV probe measurements due to acoustic phonons (Fig. S8.) However, we did not any obvious change across the spin and orbital ordering transitions (Supplementary Note 6). Both 1.0 eV and 3.1 eV pumping induce negative changes in the reflectivity change of 1.55 eV probe (Supplementary Note 7). The temperature rise due to our 1.0 eV and 3.1 eV pumping is less than 5 K[29] (Supplementary Note 8). Interestingly, we also found that the specific heat data[10] show T-dependent anomalies at all of the three spin and orbital ordering temperatures after extracting the magnetic contribution using the explicit Debye model[30] (Supplementary Note 9).

Data availability

All data generated or analysed during this study are included in this published article and its supplementary information files. The data that support the findings of this study are available from the corresponding authors upon reasonable request, in order to comply with Los Alamos National Laboratory policy on data security.

Received: 11 November 2021; Accepted: 7 December 2022;
Published online: 24 December 2022

References

1. Khomskii, D. I. Transition Metal Compounds. *Cambridge University Press* (2014).
2. Streltsov, S. V. & Khomskii, D. I. Orbital physics in transition metal compounds: new trends. *Phys.-Uspekhi* **60**, 1121 (2017).
3. Imada, M., Fujimori, A. & Tokura, Y. Metal-insulator transitions. *Rev. Mod. Phys.* **70**, 1039 (1998).
4. Caciuffo, R. et al. Resonant x-ray scattering study of magnetic and orbital order in $KCuF_3$. *Phys. Rev. B* **65**, 174425 (2002).
5. Murakami, Y. et al. Resonant X-ray scattering from orbital ordering in $LaMnO_3$. *Phys. Rev. Lett.* **81**, 582 (1998).
6. Rao, C. N. R. Charge, Spin, and orbital ordering in the perovskite manganates, $Ln_{1-x}A_xMnO_3$ (Ln = rare earth, A = Ca or Sr). *J. Phys. Chem. B* **104**, 5877 (2000).
7. Zegkinoglou, I. et al. Orbital ordering transition in Ca_2RuO_4 observed with resonant x-Ray diffraction. *Phys. Rev. Lett.* **95**, 136401 (2005).
8. Zhu, Z. H. et al. Néel and stripe ordering from spin-orbital entanglement in $\alpha - Sr_2CrO_4$. arXiv:1906.04194 (2019).
9. Jeanneau, J. et al. Magnetism and anomalous apparently inverse Jahn-Teller effect in Sr_2CrO_4. *Eur. Phys. Lett.* **127**, 27002 (2019).
10. Sakurai, H. Synthesis conditions and magnetic properties of Sr_2CrO_4 with the K_2NiF_4-type structure. *J. Phys. Soc. Jpn.* **83**, 123701 (2014).
11. Matsuno, J., Okimoto, Y., Kawasaki, M. & Tokura, Y. Variation of the electronic structure in systematically synthesized Sr_2MO_4 (M = Ti, V, Cr, Mn, and Co). *Phys. Rev. Lett.* **95**, 176404 (2005).
12. Pandey, B. et al. Origin of the magnetic and orbital ordering in $\alpha - Sr_2CrO_4$. *Phys. Rev. B* **103**, 045115 (2021).
13. Zhou, H. D., Conner, B. S., Balicas, L. & Wiebe, C. R. Orbital-ordering transition in Sr_2VO_4. *Phys. Rev. Lett.* **99**, 136403 (2007).
14. Giannetti, C. et al. Ultrafast optical spectroscopy of strongly correlated materials and high-temperature superconductors: a non-equilibrium approach. *Adv. Sci.* **65**, 58 (2016).
15. Fausti, D. et al. Light-induced superconductivity in a stripe-ordered cuprate. *Science* **331**, 189 (2011).
16. Iwai, S. et al. Ultrafast optical switching to a metallic state by photoinduced Mott transition in a halogen-bridged nickel-chain compound. *Phys. Rev. Lett.* **91**, 057401 (2003).
17. Li, T. et al. Femtosecond switching of magnetism via strongly correlated spin-charge quantum excitations. *Nature* **496**, 69 (2013).
18. Prasankumar, R. P. et al. Phase inhomogeneities in the charge-orbital-ordered manganite $Nd_{0.5}Sr_{0.5}MnO_3$ revealed through polaron dynamics. *Phys. Rev. B* **76**, 020402(R) (2007).
19. Bowlan, P. et al. Probing ultrafast spin dynamics through a magnon resonance in the antiferromagnetic multiferroic $HoMnO_3$. *Phys. Rev. B* **94**, 100404(R) (2016).
20. Prasankumar, R. P. et al. Coupled charge-spin dynamics of the magnetoresistive pyrochlore $Tl_2Mn_2O_7$ probed using ultrafast midinfrared spectroscopy. *Phys. Rev. Lett.* **95**, 267404 (2005).
21. Lee, M.-C. et al. Strong spin-phonon coupling unveiled by coherent phonon oscillations in Ca_2RuO_4. *Phys. Rev. B* **99**, 144306 (2019).
22. Coslovich, G. et al. Ultrafast dynamics of vibrational symmetry breaking in a charge-ordered nickelate. *Sci. Adv.* **3**, e1600735 (2017).
23. Ishikawa, T., Toriyama, T., Konishi, T., Sakurai, H. & Ohta, Y. Reversed crystal-field splitting and spin-orbital ordering in $\alpha - Sr_2CrO_4$. *J. Phys. Soc. Jpn.* **86**, 033701 (2017).
24. Thomsen, C., Grahn, H. T., Maris, H. J. & Tauc, J. Surface generation and detection of phonons by picosecond light pulses. *Phys. Rev. B* **34**, 4129 (1986).

25. Johnson, J. A. et al. Magnetic order dynamics in optically excited multiferroic $TbMnO_3$. *Phys. Rev. B* **92**, 184429 (2015).
26. Kurz, H., Kuett, W., Seibert, K. & Strahnen, M. Hot carrier relaxation in highly excited III-V compounds. *Solid State Electron.* **31**, 447 (1988).
27. Sugiyama, J. et al. Microscopic magnetic nature of K_2NiF_4-type 3*d* transition metal oxides. *J. Phys. Conf. Ser.* **551**, 012011 (2014).
28. Landron, S. & Lepetit, M.-B. Importance of t_{2g}-e_g hybridization in transition metal oxdies. *Phys. Rev. B* **77**, 125106 (2008).
29. Shayduk, R. & Gaal, P. Transition regime in the ultrafast laser heating of solids. *J. Appl. Phys.* **127**, 073101 (2020).
30. Debye, P. On the theory of specific heats. *Ann. der Phys.* **344**, 789 (1912).

Acknowledgements

This work was performed at the Center for Integrated Nanotechnologies at Los Alamos National Laboratory (LANL), a U.S. Department of Energy, Office of Basic Energy Sciences user facility, under user proposal 2018BU0083. It was primarily supported through the U.S. Department of Energy, Office of Science, Office of Basic Energy Sciences, Division of Materials Sciences and Engineering via FWP No. 2018LANLBES16 (M.-C.L. and R.P.P.). Work at MIT (C.O., J.L. Z.Z., and R.C.) was supported by the U.S. Department of Energy, Office of Science, Office of Basic Energy Sciences under Contract No. DE-SC0019126. Work at IOP (Z.Z.) was supported by the National Natural Science Foundation of China Under contract No.12074411.

Author contributions

M.-C.L., R.C., and R.P.P. conceived and designed the project. α-Sr_2CrO_4 single crystalline thin films were grown and characterized by J.L., Z.Z., C.O., and R.C. M.-C.L. measured the time-resolved reflectivity with help from N.S.S and L.T.M. C.O. measured reflectivity in equilibrium and S.K. transformed the data to optical conductivity using a Kramers-Kronig analysis. The data was analyzed by M.-C.L., C.O., J.L., S.K., R.C., and R.P.P. The manuscript was written by M.-C.L. and R.P.P. with significant contributions from C.O., J.L., Z.Z., R.C., and D.A.Y.

Competing interests

The authors declare no competing interests.

Additional information

Supplementary information The online version contains supplementary material available at https://doi.org/10.1038/s42005-022-01110-y.

Correspondence and requests for materials should be addressed to Min-Cheol Lee or Rohit P. Prasankumar.

Peer review information *Communications Physics* thanks Ricardo Lobo and the other, anonymous, reviewer(s) for their contribution to the peer review of this work.

Reprints and permission information is available at http://www.nature.com/reprints

Publisher's note Springer Nature remains neutral with regard to jurisdictional claims in published maps and institutional affiliations.